Predicting the June 2013 European Flooding Based on Precipitation, Soil Moisture, and Sea Level Pressure

M. IONITA

Alfred Wegener Institute Helmholtz Center for Polar and Marine Research, Bremerhaven, Germany

M. DIMA

Alfred Wegener Institute Helmholtz Center for Polar and Marine Research, Bremerhaven, Germany, and Faculty of Physics, University of Bucharest, Bucharest, Romania

G. LOHMANN AND P. SCHOLZ

Alfred Wegener Institute Helmholtz Center for Polar and Marine Research, Bremerhaven, Germany

N. RIMBU

Alfred Wegener Institute Helmholtz Center for Polar and Marine Research, Bremerhaven, Germany, and Faculty of Physics, University of Bucharest, and Climed Norad, Bucharest, Romania

ABSTRACT

Over recent decades Europe has experienced heavy floods, with major consequences for thousands of people and billions of euros worth of damage. In particular, the summer of 2013 flood in central Europe showed how vulnerable modern society is to hydrological extremes and emphasized once more the need for improved forecast methods of such extreme climatic events. Based on a multiple linear regression model, it is shown here that 55% of the June 2013 Elbe River extreme discharge could have been predicted using May precipitation, soil moisture, and sea level pressure. Moreover, the model was able to predict more than 75% of the total Elbe River discharge for June 2013 (in terms of magnitude) by also incorporating the amount of precipitation recorded during the days prior to the flood, but the predicted discharge for the June 2013 event was still underestimated by 25%. Given that all predictors used in the model are available at the end of each month, the forecast scheme can be used to predict extreme events and to provide early warnings for upcoming floods. The forecast methodology could be relevant for other rivers also, depending on their location and their climatic background.

1. Introduction

After several days of heavy rainfall, ongoing flooding in central Europe began in late May 2013. It primarily affected the southern and the eastern parts of Germany and western regions of the Czech Republic (Munich RE 2013). The flood crest then progressed down the Elbe and Danube drainage basins and tributaries, leading to high water levels along their banks. This resulted in an overall loss of more than EUR 12 billion and an insured loss in the region of more than EUR 3 billion (Munich RE 2013). Such huge damages point to an urgent need to improve the prediction methods for such extreme events.

May 2013 was the second wettest May in Germany since the beginning of observational records in ~1880 (Deutscher Wetterdienst 2013a,b). At different stations situated over the catchment area of the Elbe River, the amount of precipitation (PP) that fell during May 2013 was

---

Corresponding author address: Monica Ionita, Alfred Wegener Institute Helmholtz Centre for Polar and Marine Research, Bussestrasse 24, D-27570 Bremerhaven, Germany.
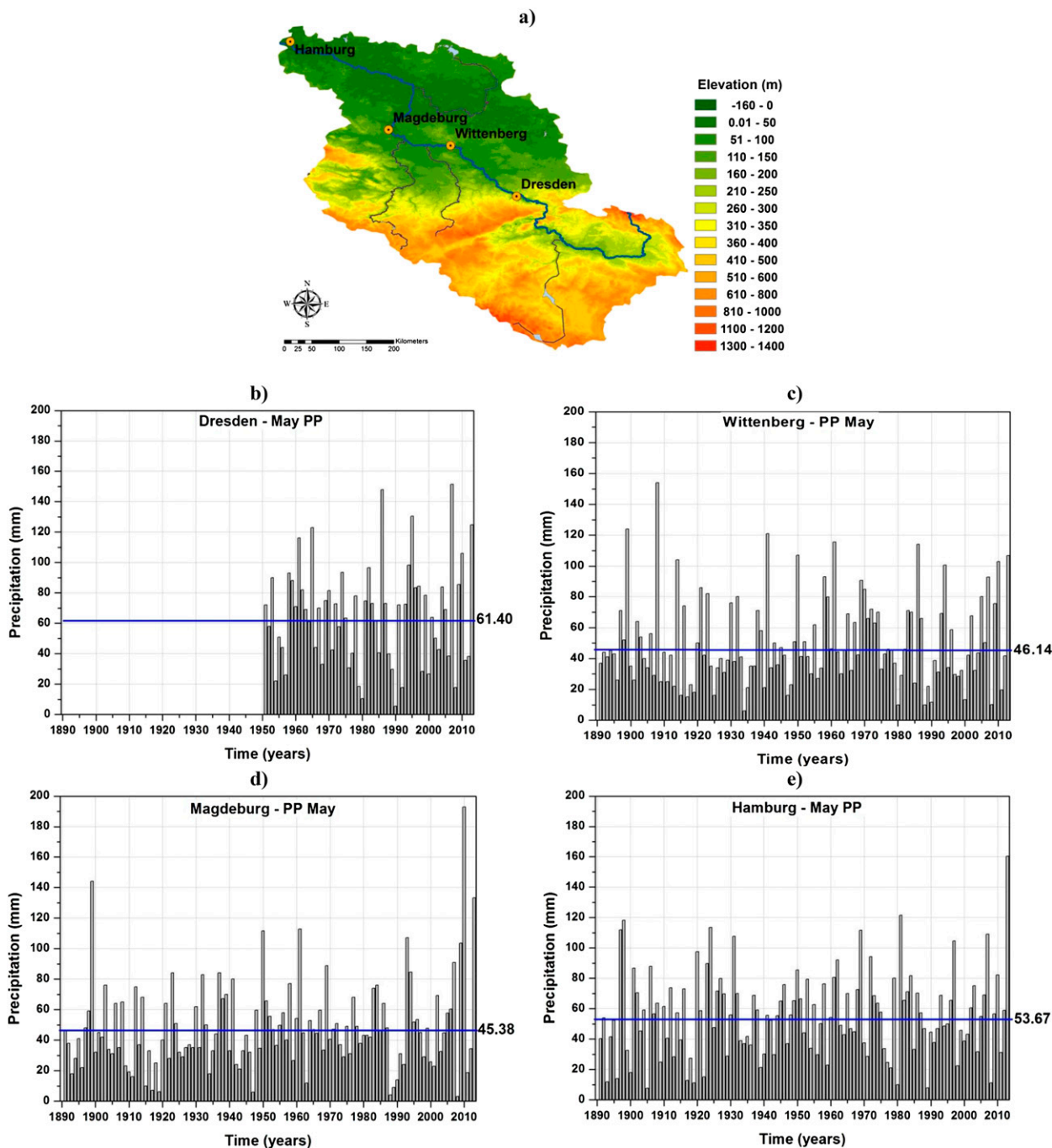E-mail: monica.ionita@awi.de

FIG. 1. Sum of May PP (mm) at different stations located over Elbe's catchment area. (a) The location of the meteorological stations in the Elbe catchment area and the sum of May PP at the (b) Dresden, (c) Wittenberg, (d) Magdeburg, and (e) Hamburg stations. The source of the PP data is Deutscher Wetterdienst (www.dwd.de). The blue line in (b)–(e) indicates the mean May PP over the period 1971–2000.

among the highest over the last 120 years (e.g., Hamburg) and more than double the May average precipitation at all the analyzed stations (Fig. 1). At basin level, the precipitation anomalies recorded in May 2013 ranged from 180 mm in the western part of the Elbe catchment area to 80–100 mm in the eastern part of the catchment area

(Fig. 2a). The average temperature in Germany in May was 11.7°C, and it was 1.3°C colder than the reference period 1981–2010 (Deutscher Wetterdienst 2013a,b). Following the late snowmelt and several wet months in spring, at the end of May 2013 the soils in the southern and eastern part of Germany had reached record levels of moisture
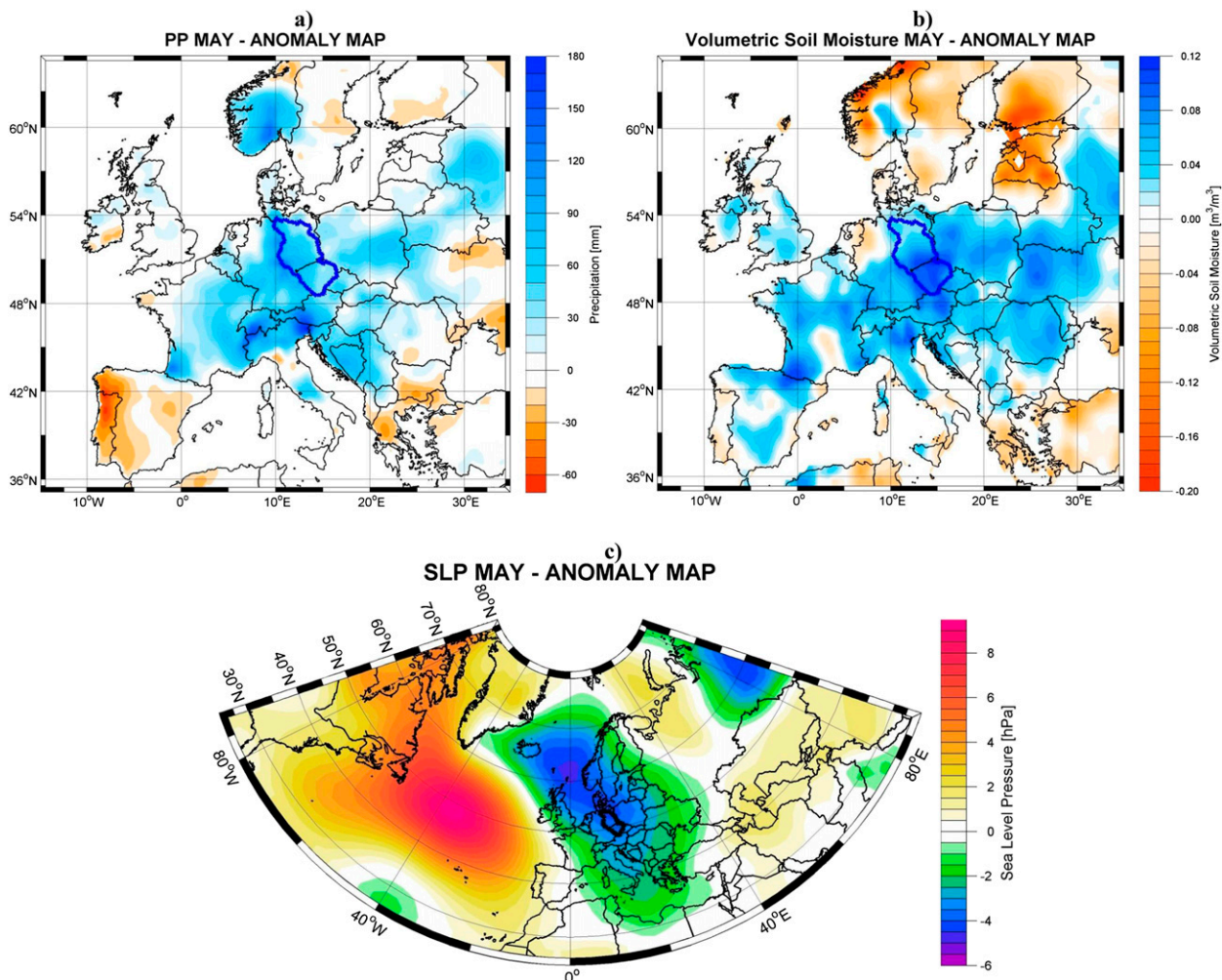
FIG. 2. (a) PP (mm; from E-OBSv8), (b) volumetric SM (fraction; from NCEP), and (c) SLP (hPa; from NCEP) anomalies for May 2013 (relative to the period 1971–2000). The area delimited by the blue line indicates the Elbe River catchment area.

(110%) that had not been observed since the first measurements in 1962 (Deutscher Wetterdienst 2013a,b). The most affected areas in the Elbe catchment area were the southern and central parts (Fig. 2b).

Major flood events result from the interaction of atmospheric and hydrological processes. Prior to major flooding, the catchment area experienced prolonged wet conditions and saturated soils. The large amount of precipitation and the saturated soil in May 2013 were the direct results of the atmospheric conditions that prevailed during this period. May 2013 was characterized by a dipole-like structure in the sea level pressure (SLP) field, characterized by an anticyclonic circulation over the central Atlantic Ocean and a cyclonic circulation over the central part of Europe and the North Sea (Fig. 2c). Moreover, the second half of May and the first days of June were characterized at the 500-mb level by an atmospheric blocking circulation that persisted for more than 16 days.

This system featured a cyclonic circulation over the Alpine region and Germany, an anticyclonic circulation over the northern part of the Scandinavian Peninsula and eastern Europe, and a cyclonic circulation over Siberia. The cyclonic circulation over the Alpine region and Germany, which is typical for spring and summer floods over central Europe and is known as "Zugstrasse Vb" (Mudelsee et al. 2004), advected a lot of moisture from the Mediterranean Sea toward the Alps.

Societies with large populations located within river watersheds use water for social purposes, agriculture, and industrial production. Therefore, streamflow forecasting is of great importance for water resource management and flood defense. Although the predictability of the seasonal streamflows is a central aspect in the investigations related to the dynamics of hydrological processes, it has received significant attention in the hydrometeorological community in recent years (Trigo et al. 2004; Rimbu et al. 2005;

Ionita et al. 2008; Gámiz-Fortis et al. 2010; Wood et al. 2002, 2005; Wood and Lettenmaier 2006). Skillful predictions can affect decision making for land and water resources management (Kirono et al. 2010).

On seasonal time scales, anomalous atmospheric circulation is often linked with seasonal variations in river discharge via variations in different climatic parameters [e.g., precipitation, temperature (TT), and soil moisture (SM)] (Dettinger and Diaz 2000; Cullen et al. 2002). For example, summer streamflow variability over the British Isles may be forecasted from prior knowledge of varying boundary conditions such as anomalous sea surface temperature (SST) in the North Atlantic Ocean (Wilby et al. 2004) and land air temperature and global teleconnection indices (Svensson and Prudhomme 2005). Wedgbrow et al. (2002) used preceding winter values of the Polar–Eurasia teleconnection pattern, North Atlantic SST, and the North Atlantic Oscillation (NAO) index to predict the upcoming summer–autumn river flow in northwestern, southwestern, and southeastern England. Ionita et al. (2008) showed that the climate information from the previous winter global SST, temperature over land, and precipitation can be used to forecast the spring streamflow variability of the Elbe River.

A different approach compared to the one used in the aforementioned studies (e.g., linear regression models) is the use of climate model–based approaches with the purpose of seasonal ensemble hydrological forecasting. In the climate model–based approach, the outputs from global climate models are downscaled to finer resolutions and bias corrected to produce the forcing for the hydrological model (Wood et al. 2002, 2005). Wood et al. (2002, 2005) conducted seasonal hydrological predictions for the eastern and western United States by bias correcting and downscaling (spatially and temporally) NCEP Global Spectral Model (GSM) ensemble climate predictions for input into the Variable Infiltration Capacity hydrologic model. They found that the initial hydrologic conditions need to be accurately determined, so that the influence of the land surface can be captured in the prediction.

Despite progress, there is still a lack of well-established methods estimating the predictability of hydrological processes based on climatic information. For example, the predictability of precipitation and streamflows in Europe based on NAO and El Niño–Southern Oscillation (ENSO) is limited because of nonstationarity (Cullen et al. 2002; Trigo et al. 2004; Rimbu et al. 2005). Also, the standard teleconnection indices are defined over specific atmospheric and oceanic regions, but the discharge of different river basins may correlate better with particular atmosphere and/or SST regions (Tootle and Piechota 2006; Ionita et al. 2008). One possibility to improve the seasonal forecast of streamflow variations would be to identify

stable predictors and develop a forecast scheme based on them. Along this line, the synoptical and climatological conditions associated with the June 2013 European floods are analyzed here in order to identify potential predictors. Further, these are placed in a longer temporal context in order to develop a prediction scheme.

2. Data and methods

a. Catchment area

The Elbe rises at an elevation of about 1400 m in the Riesengebirge on the northwest border of the Czech Republic. It is approximately 1100 km long and covers a catchment area of about 150 000 km^2 that is inhabited by 25 million people. It covers the Czech Republic and Germany and discharges into the German Bight, North Sea (Fig. 3a). The hydrological discharge regime is characterized by a pronounced seasonal cycle that has its rising limb situated between January and April and its falling one between June and September, the highest values being recorded in April. These high discharge values recorded in the spring months may be related with the melting of the snow in the catchment area and the soil humidity. The Elbe River basin is the driest basin in Germany (compared to Rhine, Weser, or Danube) because of the low precipitation levels of about 659 mm yr^{-1} on average. In May, the precipitation ranges from below 50 mm month^{-1} in the central part to 120 mm month^{-1} in the mountain area (Fig. 3b).

b. Data

The main variable analyzed in this study is the time series of Elbe River discharge. The daily values of Elbe discharge, for the period 1875–2013, recorded at the Neu Darchau gauging station (last gauging station), situated in the lower part of the Elbe catchment area (53°14'N, 10°53'E), are provided by the German Federal Institute of Hydrology [Bundesanstalt für Gewässerkunde (BfG)] in Koblenz. Neu Darchau is the only station that has available measurements until the end of June 2013. The June mean time series of Elbe streamflow includes extreme floods in 1927, 1941, 1961, 1965, 1986, and 1995, which culminated with the 2013 record value (Fig. 3c) and no significant trend (red line in Fig. 3b). The highest discharge rates occur in winter, usually reaching the North Sea from January to March/April (Fig. 3d). During the summer, less runoff is recorded.

The precipitation and temperature data from the E-OBS, version 8 (E-OBSv8), dataset (Haylock et al. 2008) are also used. The standardized precipitation index (SPI) is computed following the methodology of McKee et al. (1993) based on the precipitation from the E-OBSv8 dataset.
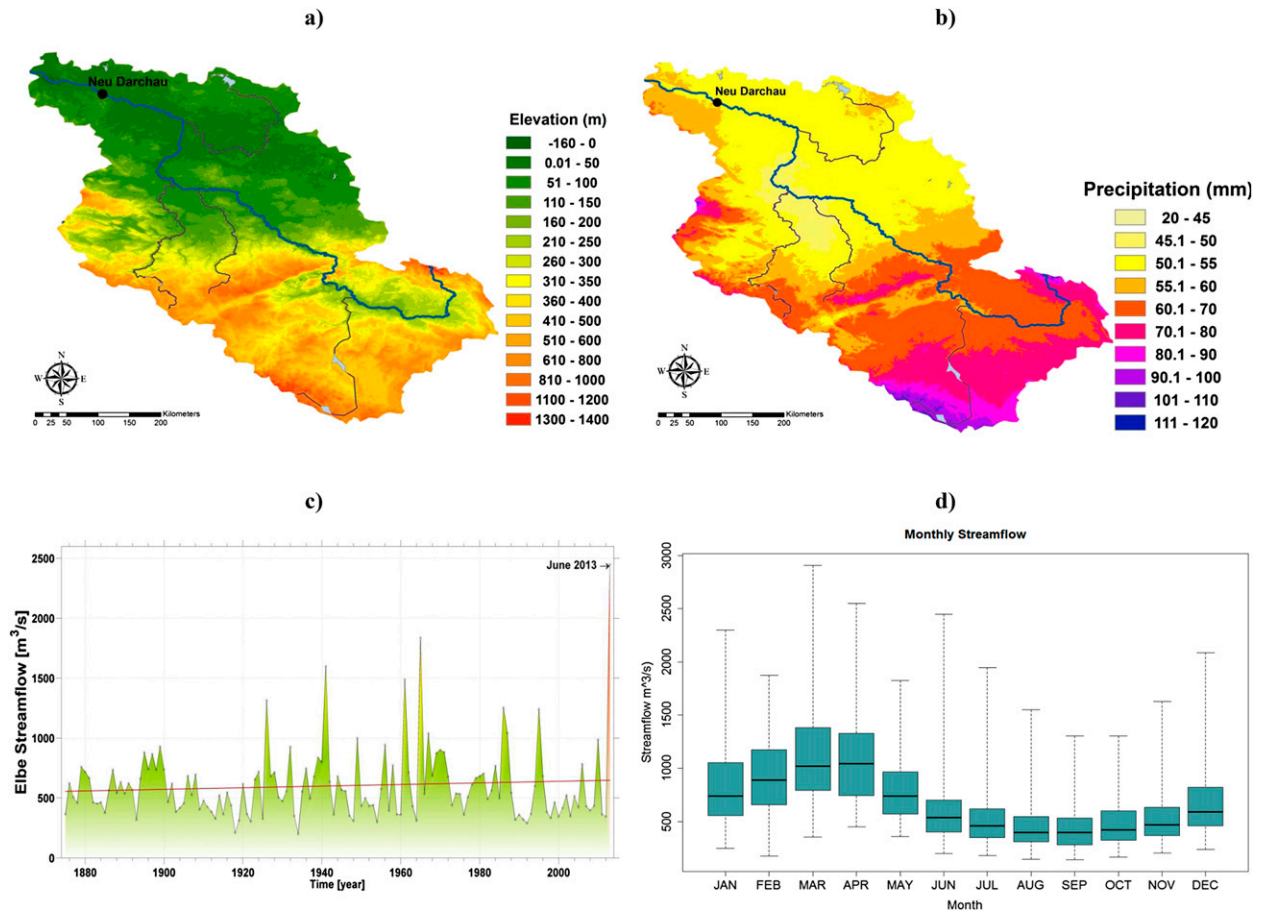
FIG. 3. (a) Topographical map of the Elbe drainage basin and Elbe River (blue line). The black dot indicates the location of the Neu Darchau station. (b) May PP climatology over the Elbe catchment area for the period 1950–2000. (c) The time series of June Elbe streamflow (filled with green) and the linear trend (red line). (d) Boxplot of Elbe climatological monthly streamflow ($m^3\,s^{-1}$) over the period 1875–2013.

These fields have a $0.25° \times 0.25°$ spatial resolution and cover the period from January 1950 to June 2013. The soil moisture, sea level pressure, relative humidity (RH), and potential evaporation rate (POT) datasets are provided by the National Center for Atmospheric Research (NCAR) and they cover the period from January 1948 to June 2013 (Kalnay et al. 1996). The volumetric soil moisture data are based on the NCEP–NCAR reanalysis product (R-1; Kalnay et al. 1996; Kistler et al. 2001). The soil moisture quantity reported here is linearly interpolated to a depth of 10 cm. The units are volumetric water content.

As a measure of local blocking frequency, we have used the two-dimensional (2D) index described by Scherrer et al. (2006). It is an extension of the one-dimensional Tibaldi–Molteni index (Tibaldi and Molteni 1990) to a two-dimensional map of blocking frequencies at every grid point. For each grid point the southern gradient (GHGS) and the northern gradient (GHGN) are evaluated as follows:

$$\mathrm{GHGS} = [Z(\phi_0) - Z(\phi_0 - 15°)]/15° \quad \text{and}$$
$$\mathrm{GHGN} = [Z(\phi_0 + 15°) - Z(\phi_0)]/15°$$

where ϕ_0 is the latitude of the considered grid point.

For each May we calculate the ratio between the number of days when a certain grid point was blocked, that is, the conditions GHGS > 0 and GHGN < [(−10 m)/(°lat)] are simultaneously satisfied for at least five consecutive days.

The dataset used in this study to calculate the 2D blocking frequency is based on the daily 500-hPa geopotential height Z500 extracted from the Twentieth Century Reanalysis database (Whitaker et al. 2004; Compo et al. 2006, 2011).

To evaluate the skill of the forecast to different soil moisture datasets, we make use in this study of three different soil moisture datasets. The most used reanalysis products, which also comprise soil moisture datasets, are 1) ERA-Interim data (Dee et al. 2011), 2) NASA Modern-Era Retrospective Analysis for Research and

Applications (MERRA) data (Rienecker et al. 2011), and 3) the NCEP–NCAR 40-yr reanalysis project (Kalnay et al. 1996). ERA-Interim is the latest reanalysis dataset from the European Centre for Medium-Range Weather Forecasts (ECMWF). The land surface scheme has a global coverage with a T159 horizontal resolution and four layers of soil moisture corresponding to depths of 7, 21, 72, and 189 cm. ERA-Interim extends over the period from 1979 to present. MERRA provides the second generation of reanalysis data from NASA and uses the GEOS, version 5 (GEOS-5), catchment land surface model. The model includes a latitude–longitude horizontal resolution of $0.5° \times 0.33°$ and two vertical layers: a 0–2-cm surface layer and a "root zone" layer that extends from the surface to the depth Z_R, with $75 \leq Z_R \leq 100$ cm depending on local soil conditions (Reichle et al. 2011). MERRA also has a temporal coverage from 1979 to present. The NCEP–NCAR reanalysis product was the first analysis product used in scientific research and is still frequently used. Here we use the R-1 version (Kalnay et al. 1996; Kistler et al. 2001), which has a temporal coverage from 1948 to present. R-1 is based on the Oregon State University (OSU) land surface model (Pan and Mahrt 1987). The soil column consists of two soil layers of constant thickness: 0–10 and 10–200 cm. The soil moisture quantities reported here are all linearly interpolated to a depth of 10 cm for each reanalysis dataset. The units are volumetric water content.

c. Methods

The forecast scheme for monthly Elbe River streamflow is based on a methodology similar to that used for seasonal prediction of Danube River flow (Rimbu et al. 2005) and for the seasonal prediction of spring Elbe streamflow (Ionita et al. 2008). The basic idea of this procedure is to identify regions with stable teleconnections between the predictors and the predictand (Lohmann et al. 2005). The June streamflow anomalies have been correlated with the potential predictors from the previous month (May) in a moving window of 21 years. The results remain qualitatively the same if the length of the moving window varies between 15 and 40 years. The correlation is considered to be stable for those grid points where June streamflow and May PP, volumetric SM, SLP, TT, SPI, POT, and RH anomalies are significantly correlated at the 90% level ($r = 0.25$) or 80% level ($r = 0.20$) for more than 80% of the 21-yr windows, covering the period 1950–2013. The regions where correlation is positive and stable at the 90% (80%) level will be represented as red (yellow) on a global map. The regions where correlation is negative and stable at the 90% (80%) level are represented as blue (green). Such maps will be referred to in our study

as stability correlation maps, and their structures remain qualitatively unchanged if the significance levels that define the stability of the correlation vary within reasonable limits. We have also adopted a different approach to choose just the optimal predictors identified by the stability maps. Previous studies (Rimbu et al. 2005; Ionita et al. 2008) use the first principal component based on all the stable indices as a potential predictor. Here, the optimal model is established based on a multiple regression analysis of the stable predictors.

d. Model evaluation

The skill of forecast models can be assessed through several methods (Wilks 1995; von Storch and Zwiers 1999). In this paper we use three measures of the forecast model skill: 1) the percentage improvement in the root-mean-square error RMSE over a climatological forecast $\text{RMSE}_{\text{clim}}$ and over persistence $\text{RMSE}_{\text{pers}}$, 2) the coefficient of variation (CV; Alfieri et al. 2013), and 3) the Wilcoxon test.

1) The RMSE skill measure is one of the most robust. Climatology is taken as the standardized long-term average prior to each forecasted year, while persistence is taken as June Elbe streamflow. We computed the skill score (SS) (Wilks 1995), defined as

$$\text{SS} = 1 - \frac{\text{RMSE(forecast)}}{\text{RMSE(reference forecast)}},$$

where the reference forecast is either climatology or persistence. The skill score has the value of one for perfect forecasts and zero if the forecasts are no better than the reference one and is unbounded below zero for forecasts that are worse than the reference one.

2) The coefficient of variation is a dimensionless indicator that enables a direct comparison between the forecasted and observed values, without being affected by any bias of estimation. CV is defined as

$$\text{CV} = \frac{\sigma(Q_{\text{sim}} - Q_{\text{obs}})}{Q_{\text{obs}}},$$

where Q_{sim} is the simulated streamflow, and Q_{obs} is the observed streamflow.

3) The Wilcoxon test is a nonparametric test designed to evaluate the difference between two treatments or conditions where the samples are correlated.

3. Results

a. Meteorological conditions prior to the June 2013 flood

Among potential predictors, atmospheric blocking is an important candidate and has already been associated

with extreme weather events like floods, droughts, heat waves, or cold surges (Scherrer et al. 2006; Sillmann and Croci-Maspoli 2009). This process is one of the most prominent features of the midlatitude low-frequency atmospheric variability. The 2013 extreme event was triggered by a typical atmospheric circulation for summer floods. The second half of May and the first days of June were characterized by an atmospheric blocking circulation that persisted for more than 16 days (Fig. 4a). This system featured a cyclonic circulation over the Alpine region and Germany, an anticyclonic circulation over the northern part of the Scandinavian Peninsula and eastern Europe, and a cyclonic circulation over Siberia. This stationary regime led to the blocking of several synoptic systems, like the Azores high and the Siberian anticyclone, which extended southwest of its normal position, thus blocking the eastward progression of the central European low. The cyclonic circulation over the Alpine region and Germany, which is typical for spring and summer floods over central Europe, forced a lot of moisture advection from the Mediterranean Sea toward the Alps. In a longer-term perspective, June high streamflow events are associated with a similar blocking-like circulation (Fig. 4b). Based on a 2D blocking index (Scherrer et al. 2006), we show that high streamflow anomalies, over the period 1875–2013, are occurring in association with an omega type of atmospheric blocking (two cutoff lows and one blocking high that form the Greek letter omega; Rex 1950). For most of the omega blocks, the western low (in our case the low centered over the Mediterranean Sea and the Alpine region) produces heavy precipitation. Because of the astounding longevity of some omega blocks and their spatial extent, flooding conditions that may occur with this kind of block can be severe. Usually, a center of anticyclonic circulation over Scandinavia is flanked by a center of low pressure over eastern Europe, which allows a lot of moisture to be advected from the Mediterranean region toward the Alps and Germany, inducing high rates of precipitation. Through their persistence over the same region for a significant number of days, these atmospheric conditions favor the generation of extreme events (e.g., heavy precipitation and floods).

b. Selection of potential predictors

The skill of a long-range forecast is associated with the predictors that represent the slow varying components of the climate system such as sea ice, snow cover, soil moisture, and SST (Koster et al. 2010). Most of the streamflow predictors are based on meteorological parameters or SSTs (Rimbu et al. 2005; Ionita et al. 2008; Gámiz-Fortis et al. 2010). Because the soils in Germany
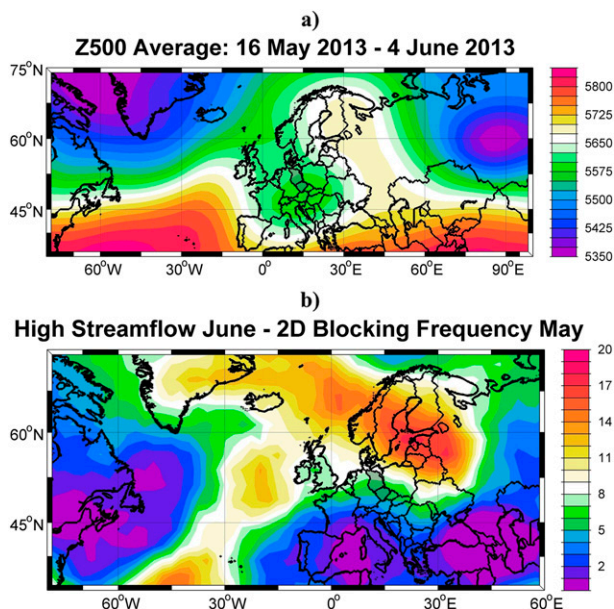

FIG. 4. (a) The synoptic situation in terms of Z500 (mb) for the period from 16 May to 4 Jun 2013. (b) The 2D blocking frequency (16–31 May) associated with June high streamflow anomalies (more than one std dev) for the period 1875–2013 (given as the percentage of blocked days relative to the total number of days).

had reached record levels of moisture prior to the June floods, in this paper we aim to analyze the potential of soil moisture as a predictor, together with the meteorological parameters. The information related to this type of predictor also has the potential to improve seasonal precipitation prediction (Dirmeyer and Brubaker 1999; Reichle and Koster 2003), whereas different studies suggest that it can also substantially improve streamflow prediction (Berg et al. 2006; Koster et al. 2010). According to a number of observation-based studies, soil moisture memory can have a time scale of 1–3 months (Vinnikov and Yeserkepova 1991), thus providing some indication of the conditions prior to the forecasted month or season. As a result, here we investigated a potential link between saturated, wet, cold springs and upcoming floods.

Since PP and TT have a significant influence on streamflows, we consider them, together with SLP, SM, RH, SPI for one accumulation period of 3 months (SPI3), and POT as possible predictors for the Elbe River discharge. To identify possible links between these predictors and Elbe streamflow, stability correlation maps (see section 2c for definition) are calculated between the June discharge time series and May PP, TT, SM, SLP, SPI3, RH, and POT.

The stability correlation map between June streamflow and May PP (Fig. 5a) indicates just one significant
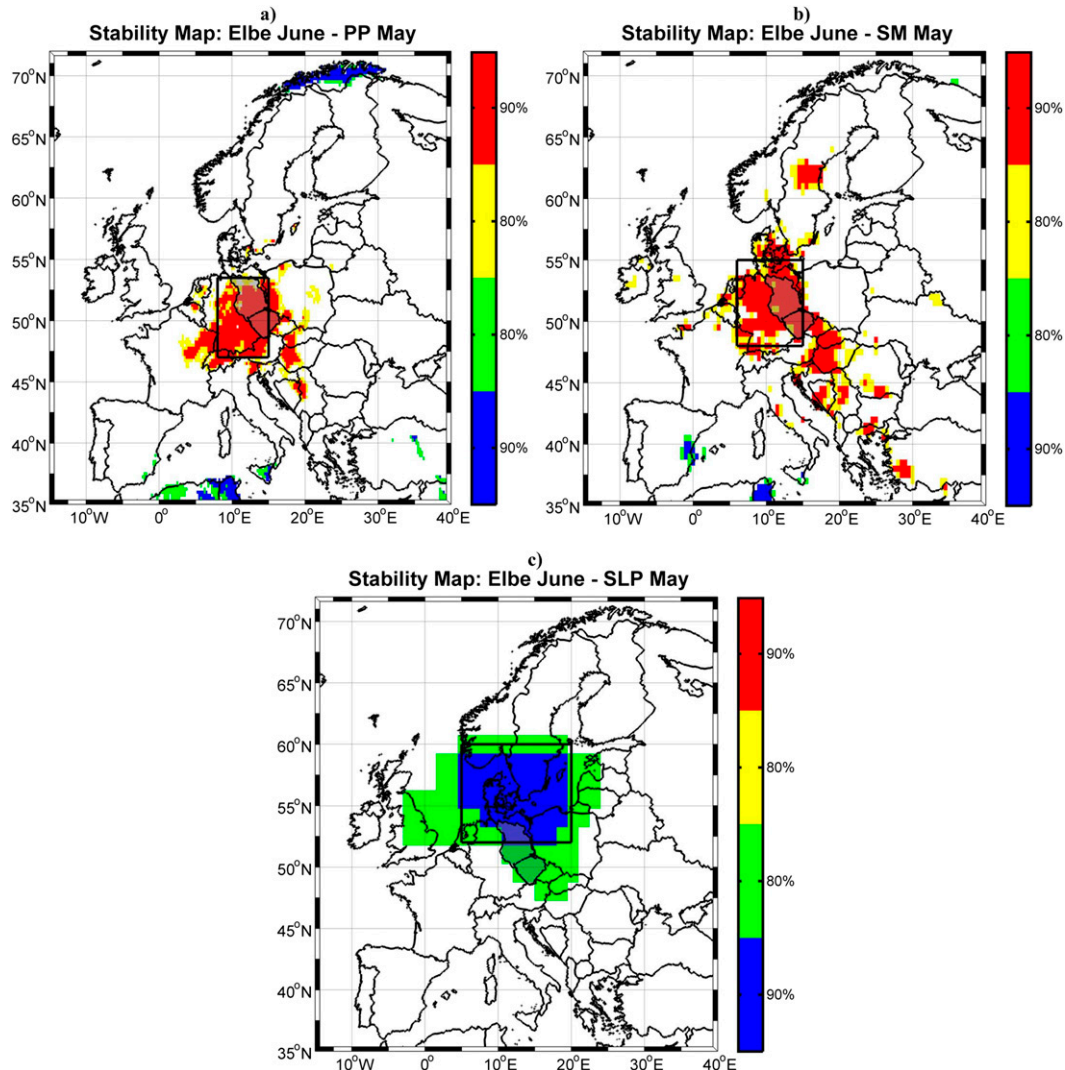
FIG. 5. Stability map of the correlation between June streamflow and May (a) PP, (b) SM, and (c) SLP. Regions where the correlation is stable, positive, and significant at the 90% (80%) level for at least 80% windows are shaded with red (yellow). The corresponding regions where the correlation is stable, but negative, are shaded with blue (green).

stable region, which covers most of Germany. Based on this, we define an index as the May PP averaged over the region (47°–53.5°N, 7.5°–15°E) as a stable predictor for June Elbe streamflow. The correlation coefficient between this index and the June streamflow time series is $r = 0.65$ (99.9% significance level) for the 1950–80 period. As in the case of precipitation, the stability map between June streamflow and May SM (Fig. 5b) indicates as a potential predictor a region centered over the whole German territory. Consequently, an index is defined as the average May soil moisture values for the region (48°–55°N, 6°–15°E). The correlation coefficient between June streamflow and SM index is $r = 0.59$ (99.9% significance level). Similarly, a region of negative and

stable correlations over the North Sea and the surrounding areas is identified in the stability map for the June Elbe streamflow and May SLP (Fig. 5c). Based on this map, an index is defined as the average SLP values over the region (52.5°–60°N, 0°–20°E) and is considered as a potential predictor for June streamflow. The correlation coefficient between June streamflow and SLP index is $r = -0.42$ (95% significance level). The stability correlation map for the June Elbe streamflow and May TT (Fig. 6a) includes an area of prominent values extending over the southern part of the Scandinavian Peninsula. Consequently, the TT index is defined by averaging TT anomalies over the area (59°–62°N, 9°–15°E). The correlation between the TT index and the
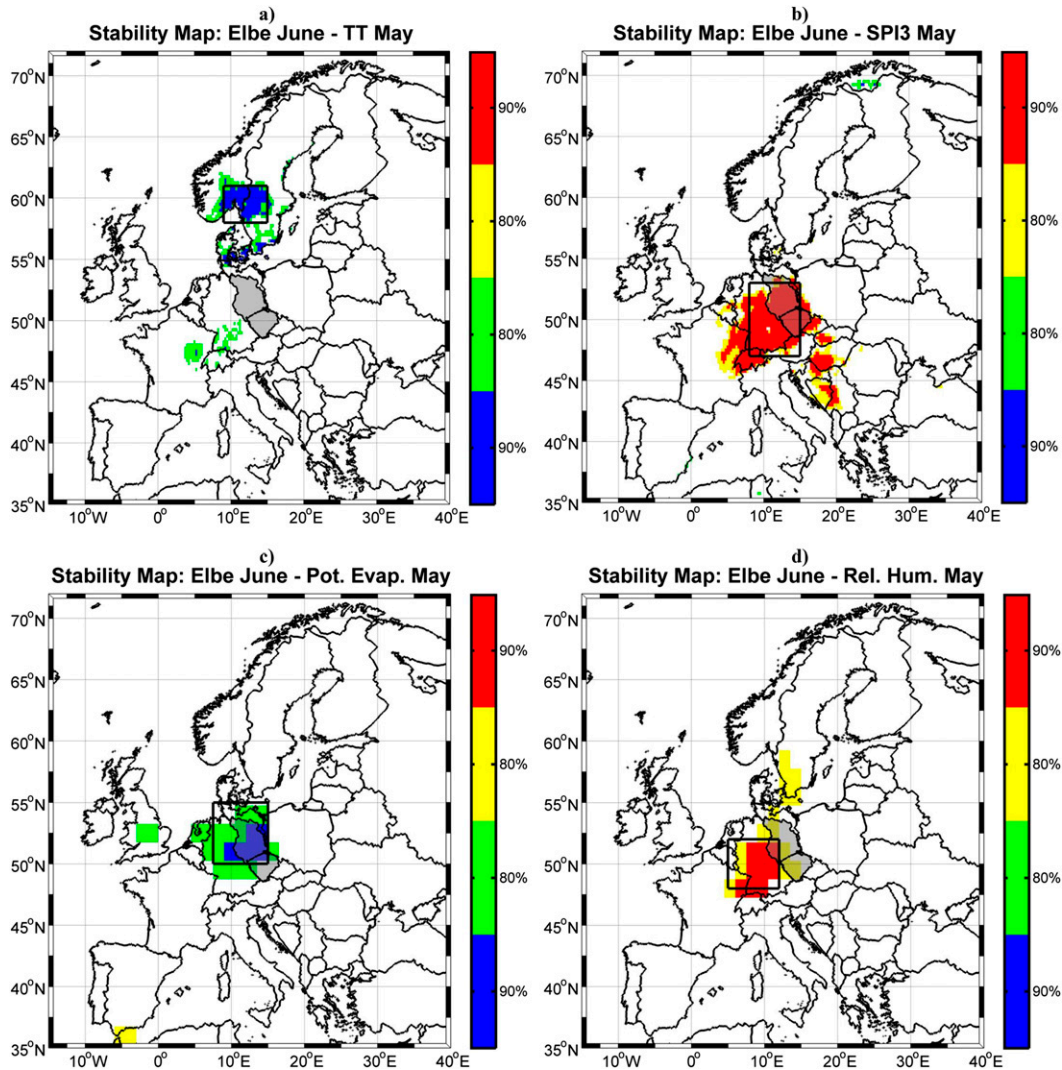
FIG. 6. Stability map of the correlation between June streamflow and May (a) TT, (b) SPI3, (c) POT, and (d) RH. Regions where the correlation is stable, positive, and significant at the 90% (80%) level for at least 80% windows are shaded with red (yellow). The corresponding regions where the correlation is stable, but negative, are shaded with blue (green).

streamflow time series is $r = -0.41$ (95% significance level). Similar stability maps have been produced for SPI3 (Fig. 6b), POT (Fig. 6c), and RH (Fig. 6d). For SPI3, an index has been defined over the region (47°–53°N, 8°–15°E), for POT over the region (50°–55°N, 7.5°–155°E), and for RH over the area (48°–52°N, 6°–12°E). The correlation coefficients between SPI3, RH, and POT and June streamflow are $r = 0.49$ (99% significance level), $r = 0.39$ (95% significance level), and $r = -0.44$ (95% significance level), respectively.

TABLE 1. Calibration statistics for the forecast model (1950–80).

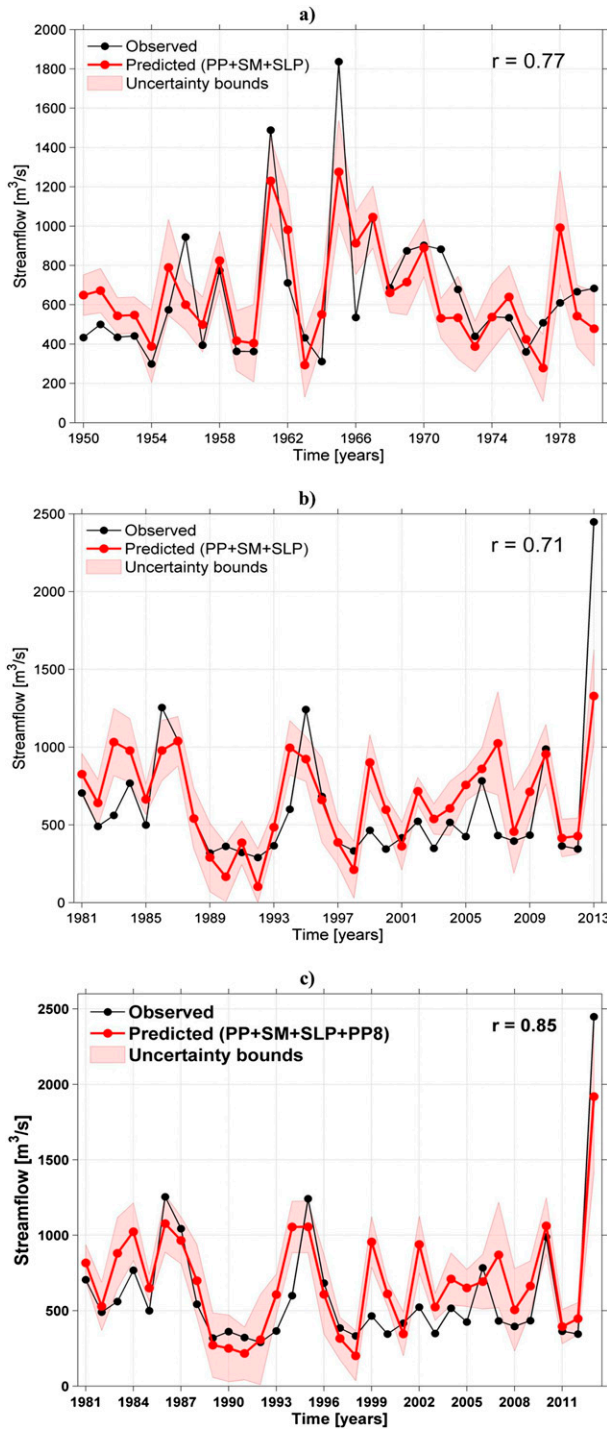| Model	Explained variance (%)	R^2	F statistic	P value	AIC	Residual std error
PP + SM + TT + RH + POT + SPI3 + SLP	51.9	0.6029	7.157	3.19×10^{-5}	451.22	225.0
PP + SM + TT + POT + SPI3 + SLP	53.1	0.6013	8.547	1.08×10^{-5}	449.38	221.1
PP + SM + TT + SPI3 + SLP	54.0	0.5978	10.40	3.56×10^{-6}	447.74	219.9
PP + SM + SPI3 + SLP	54.3	0.5883	12.86	1.34×10^{-6}	446.5	219.3
PP + SM + SLP	54.7	0.5809	17.09	3.96×10^{-7}	445.3	218.3

FIG. 7. Comparison between the observed and predicted streamflow values. (a) Observed (black) and predicted (red) June streamflow values for the calibration period 1950–90 based on May (PP + SM + SLP) from the stable regions. (b) As in (a), but for the validation period 1991–2013. The shaded area represents the 95% uncertainty bounds. (c) As in (b), but taking into account also the precipitation fallen in the first 8 days of June 2013.

TABLE 2. Test results for the comparison between forecasted and observed streamflow at 95% confidence level.

Model	S_{clim} (%)	S_{pers} (%)	CV	RMSE	Wilcoxon P value
PP + SM + SLP	43	42	0.49	10.24	0.05

c. Forecast model and streamflow prediction

Based on the May indices defined above (PP, SLP, SM, TT, SPI3, RH, and POT), a forecast scheme for June streamflow is developed based on multiple linear regression. The time interval 1950–80 is considered as the calibration period and the prediction is validated over the time interval 1981–2013. A model is constructed using the May indices over the calibration period as predictors for June streamflow. The forecast is performed by combining different predictors. Stepwise and backward regression is used in order to identify the predictors that play the most significant role for predicting the June streamflow. To estimate possible overfitting, the Akaike information criterion (AIC; von Storch and Zwiers 1999), the explained variance, R^2, and the residual standard error (Table 1) are used to choose the optimal model for explaining the June streamflow. Based on these methods, the optimal model explaining June streamflow is based on a combination of PP, SLP, and SM indices. The explained variance of this model is 54%. By including the TT, RH, SPI3, and POT indices as potential predictors, the model does not improve its predictive skill. The optimal model for explaining June Elbe streamflow (ES) is given by the following equation:

$$ES = a + bSLP(hPa) + cPP(mm\,month^{-1})$$
$$+ dSM(m^3\,m^{-3}),$$

where $a = -33\,615$ (dimensionless), $b = 31.9$ (hPa), $c = 28.58$ (mm month^{-1}), and $d = 3.517$ (m^3 m^{-3}).

The correlation coefficient between the observed and the modeled time series is $r = 0.77$ (calibration period; Fig. 7a) and $r = 0.71$ (validation period; Fig. 7b). To better assess the skill of the forecast, the RMSE, the CV, the skill score against climatology S_{clim} and persistence S_{pers}, and the Wilcoxon test are calculated (Table 2). The model exhibits a forecast skill that is 43% (42%) better than that based on climatology (persistence). Results reveal a good skill (Table 2) with a significant correlation coefficient between the raw series and the forecasted values ($r = 0.71$). The forecast model presents a small coefficient of variation (CV = 0.49), implying a variability of the predicted values lower than the observed discharge. The P value of the Wilcoxon test is
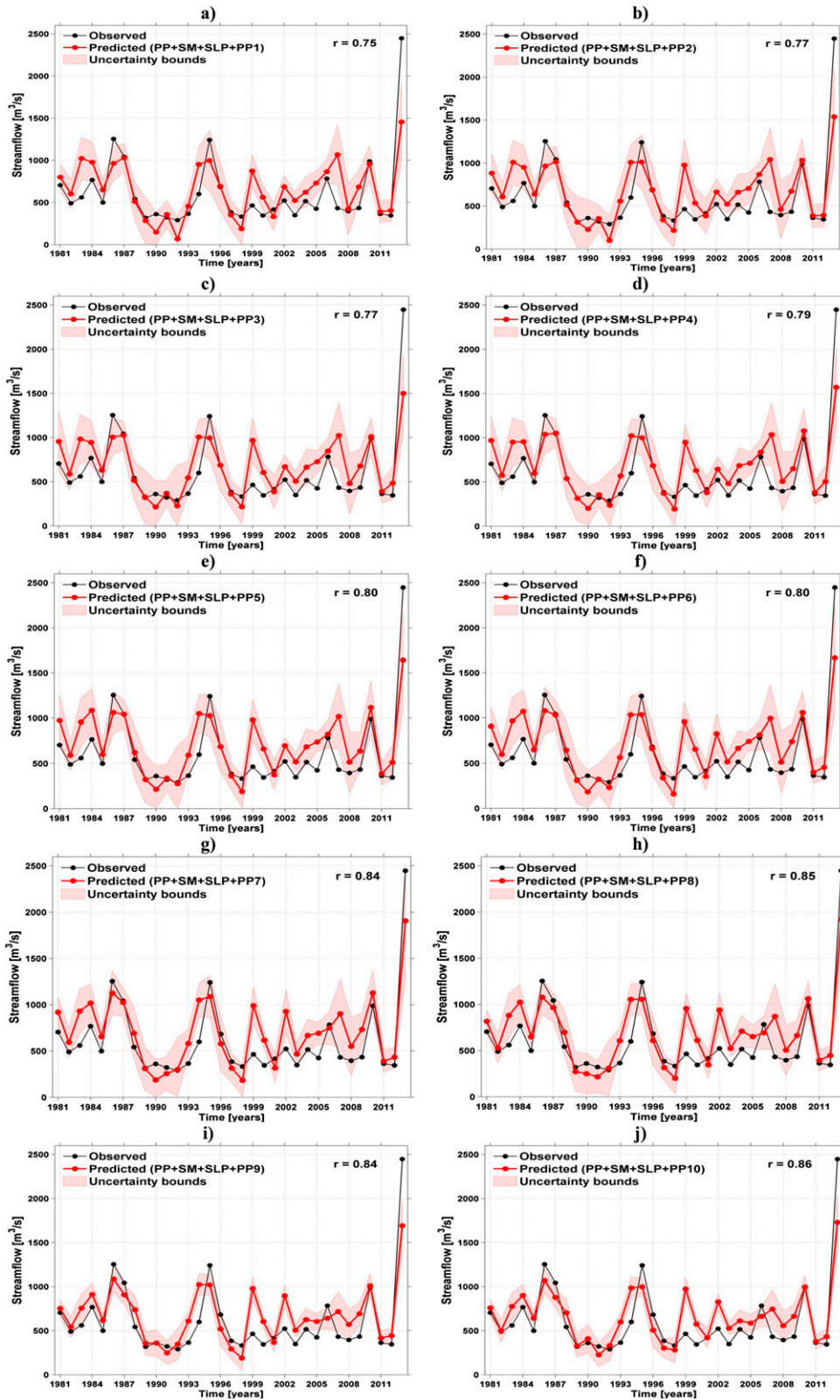
FIG. 8. Observed (black) and predicted (red) June streamflow anomalies (red line) for the validation period 1991–2013 based on May (PP + SM + SLP) together with June PP (1–10 Jun) from the stable regions. PP1 refers to the precipitation fallen on the first day of June, PP2 refers to the sum of precipitation fallen on the first and second day of June, and so on.

This demonstrates that there are no significant differences between the observed and forecasted mean.

d. Extreme floods and heavy precipitation

The extreme events, especially those that are the result of heavy precipitation, cannot be predicted based only on conditions of the previous month (or season). As a consequence, one should also consider as a predictor the precipitation that fell every day prior to the flood. The daily PP prior to the floods is an important predictor, especially when the background conditions are an indicator for possible floods, as was the case for the June 2013 flood. The atmospheric conditions for the period of mid-May until the beginning of June 2013 (Figs. 2, 4a) represented a clear indication for heavy precipitation. To prove this, we apply stepwise integration of the precipitation that fell during the days prior to the flood and show in Fig. 7c the potential predictability of the June 2013 flood by taking into account the precipitation that fell between 1 and 10 June. The highest observed discharge was recorded on 12 June 2013. As it can be inferred from Fig. 8, the predictability of this extreme flood is the highest after integrating the 8 June precipitation into the forecast scheme (Figs. 7c, 8h), with 75% of the June 2013 event amplitude predicted by the model. Although our model was able to predict more than 75% of the total Elbe River discharge for the June 2013 flood (in terms of magnitude), the predicted discharge for this particular event was still underestimated by 25%. Nevertheless, for this year our model did predict the highest discharge over the validation period.

4. Comparison with ERA-Interim and MERRA volumetric soil moisture data

Soil moisture can have a substantial influence on the climate system, as it acts as a memory for climatic anomalies (Manabe and Delworth 1990; Delworth and Manabe 1993). However, because of the difficulty of making real-time observations for this quantity, many studies based on it are performed on reanalysis high-resolution data, instead of observational fields. The lack of soil moisture observations has led researchers to depend on model-estimated values in various studies, including climate modeling, water resources management, and seasonal prediction (Mahanama et al. 2008; Koster et al. 2010). Although the reanalysis products combine numerical modeling and satellite observations through data assimilation, uncertainty remains in several variables, including soil moisture (Berg et al. 2003; Zhao et al. 2006). To evaluate the sensitivity of the forecast skill to different soil moisture datasets, we show the results for the Elbe River streamflow forecast based on
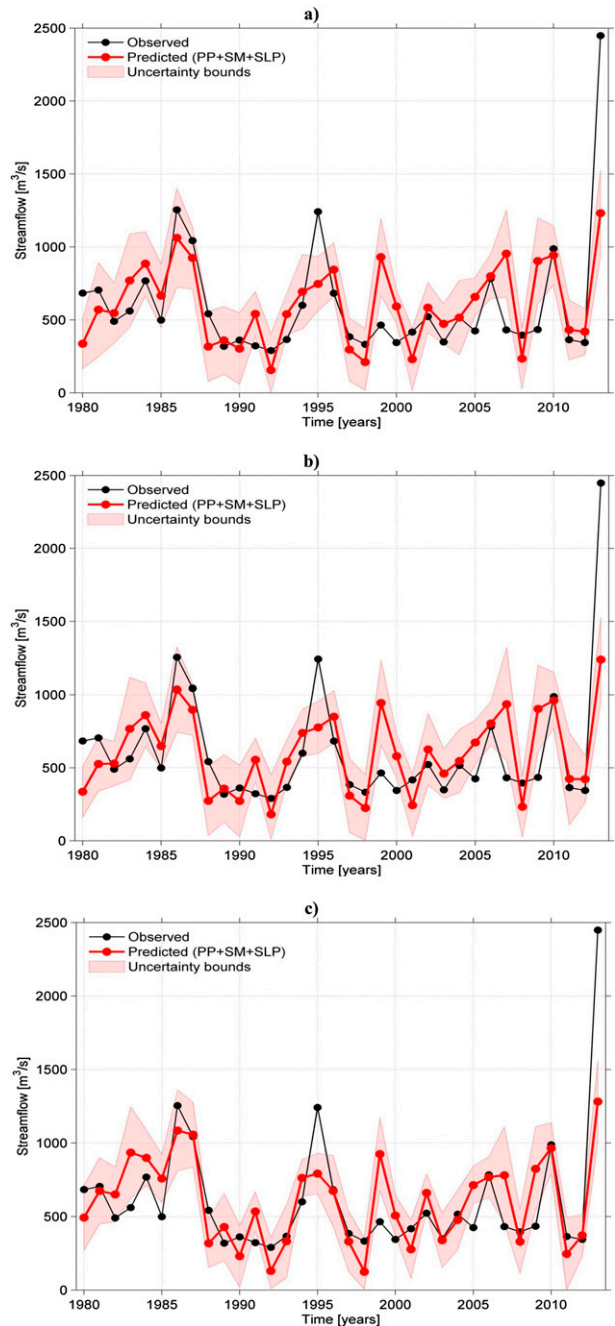

FIG. 9. Comparison between the observed (black) and predicted (red) June streamflow values based on the (a) NCEP volumetric SM, (b) ERA-Interim, and (c) MERRA data. The shaded area represents the 95% uncertainty bounds.

three different soil moisture data: NCEP, ERA-Interim, and MERRA.

The forecast of June streamflow based on the comparison of the aforementioned three datasets is shown in Fig. 9 and the statistic measures for the forecast model are shown in Table 3. Based on the information in Table 3,

TABLE 3. Statistics for the forecast model based on ERA-Interim, MERRA, and NCEP data.

	Explained variance (%)	R	R^2	F statistic	P value	Residual std error
ERA-Interim	40.3	0.67	0.44	7.98	4.653×10^{-4}	323.3
MERRA	45.9	0.71	0.51	10.43	7.325×10^{-5}	303.3
NCEP	39.3	0.67	0.44	8.01	4.542×10^{-4}	323.0

the MERRA soil moisture shows a better skill for the streamflow forecast, when compared to ERA-Interim and NCEP data. All the statistical parameters used to test the model skill (e.g., explained variance, R, R^2, and the residual standard error) show an improved skill for the MERRA dataset. The differences between ERA-Interim and NCEP fields are not significant. These results indicate that the forecast skill may depend on the used dataset.

Depending on the climatological background and on the availability of observational data, different datasets can perform better over particular regions compared to other datasets. For example, over eastern China the ERA-Interim data are the best in describing the soil moisture, precipitation, and evapotranspiration climatology compared to MERRA and NCEP data (Liu et al. 2014). Therefore, for streamflow (or other variable) prediction,
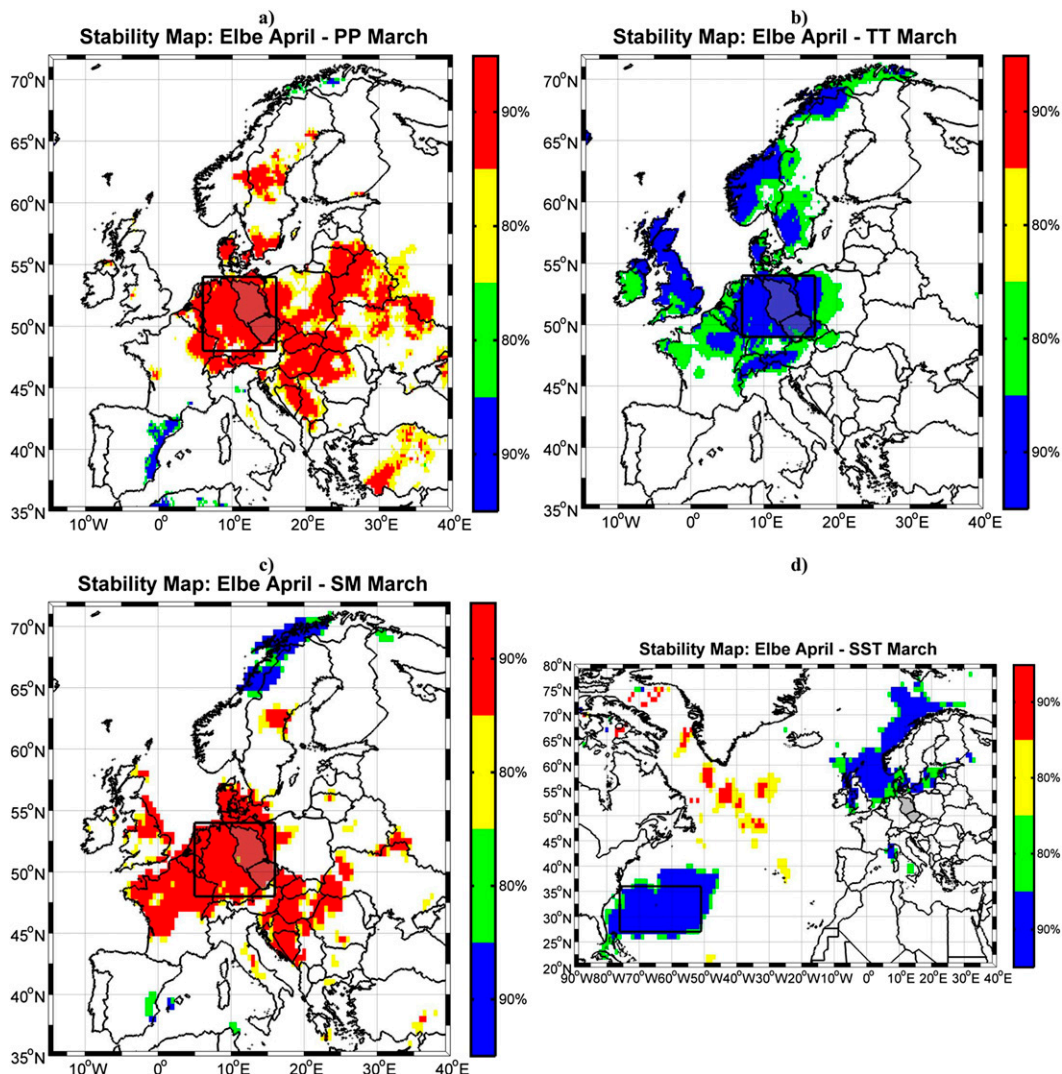

FIG. 10. Stability map of the correlation between April streamflow and March (a) PP, (b) TT, (c) SM, and (d) SST. Regions where the correlation is stable, positive, and significant at the 90% (80%) level for at least 80% windows are shaded with red (yellow). The corresponding regions where the correlation is stable, but negative, are shaded with blue (green).
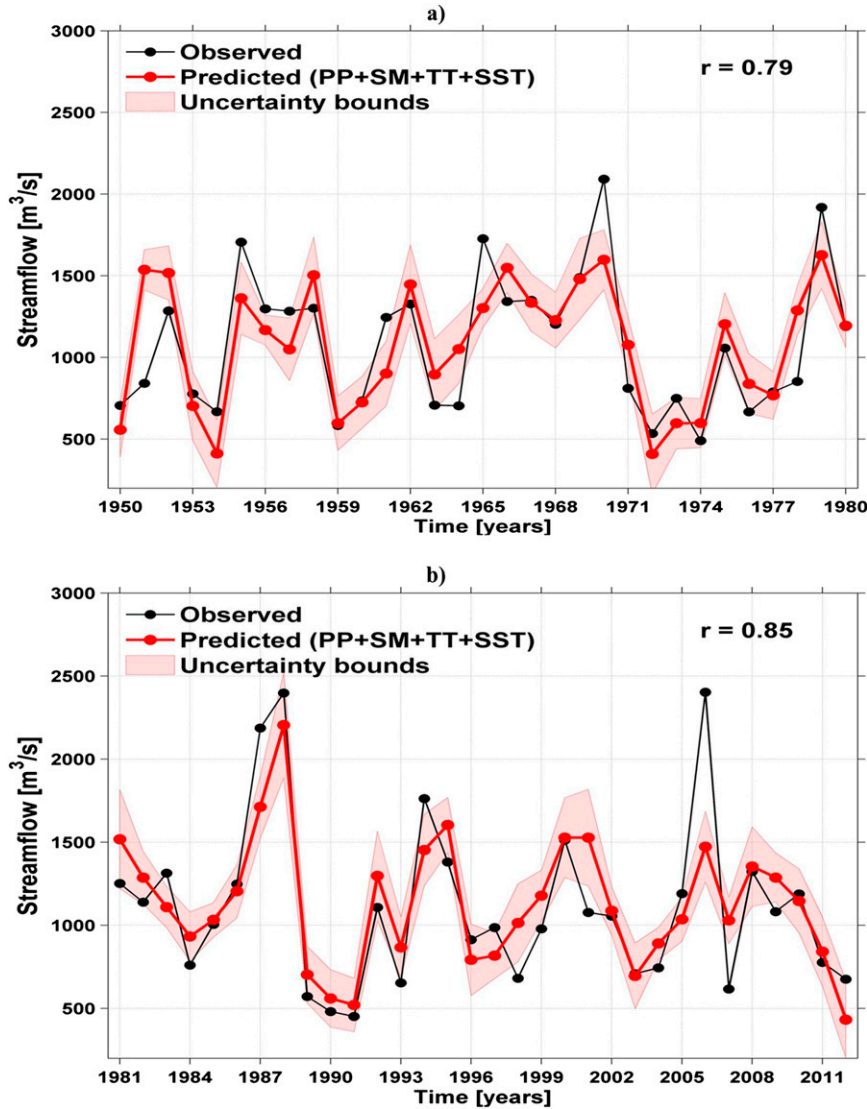
FIG. 11. Comparison between the observed and predicted streamflow values: observed
(black) and predicted (red) April streamflow values for the (a) calibration period 1950–80
based on March (PP + SM + TT + SST) from the stable regions identified in Fig. 10 and
(b) validation period 1981–2012 based on March (PP + SM + TT + SST) from the stable
regions identified in Fig. 10.

one should consider all the available datasets and choose,
based on the skill of the forecast model, the best dataset.

5. Transferability of the method

Although the aim of the current study was to focus on
the predictability of the June Elbe streamflow, we also
decided to test the applicability of this methodology for
other months. Depending on the size of the catchment
area and on the climatic context/background, the opti-
mal predictors can differ from one month to another.
For example, in the case of winter months, the snow

cover and the sea surface temperature can play a signif-
icant role for the upcoming spring floods. To emphasize
this aspect and the fact that the methodology has the
ability to be transferable to other months also, we show
here the potential predictability of April streamflow
based on the conditions of previous months. Following
the same steps as in the case of the June streamflow,
different predictors have been tested (e.g., sea level
pressure, precipitation, temperature, soil moisture, sea
surface temperature, relative humidity, and standard-
ized precipitation index). For each of the aforemen-
tioned predictors, we computed the stability maps. In

Fig. 10 we show the stability maps between April streamflow and March PP (Fig. 10a), TT (Fig. 10b), SM (Fig. 10c), and SST (Fig. 10d). After applying stepwise and forward multiple regression analysis, only the PP, TT, SM, and SST indices have been considered for the forecast scheme.

The correlation coefficient between the observed and the modeled time series is $r = 0.79$ (calibration period; Fig. 11a) and $r = 0.85$ (validation period; Fig. 11b). As in the case of June streamflow, some extreme events (e.g., year 2006) could not be fully predicted just taking into account the previous month's conditions. The high streamflow recorded in April 2006 was the result of snowmelt and intense precipitation that fell at the beginning of April (Belz et al. 2006). As in the case of June 2013, to be able to predict the actual magnitude of the recorded streamflow, one needs to also consider the precipitation that fell in the days prior to the flood. There are also cases when the extreme floods, in spring months, are just the result of snowmelt and saturated soil. This was the case of April 1988 (Puffahrt 2008). The highest discharge recorded over the period 1950–2012 was in April 1988. Almost 100% of the amplitude of this extreme event was forecasted by our model because it was the direct result of the previous month's conditions. Therefore, a specific model should be constructed for each month and for every specific location.

6. Discussion and conclusions

Since most of the extreme floods over Elbe's catchment area occurred during summer months (e.g., August 2002 and June 2013), it is necessary to identify stable predictors from antecedent months (e.g., May) that can be used to predict the floods with a certain degree of accuracy. By using a simple, but efficient methodology, we showed that at least 54.3% of the magnitude (observed versus predicted) of the June 2013 streamflow could have been predicted at the end of May 2013, based on antecedent conditions, and that more than 75% of the magnitude (observed versus predicted) could have been predicted, if precipitation values recorded several days in advance had also been used.

As shown in Fig. 8, the model is strongly dependent on the availability of near-real-time data of precipitation, especially for summer months characterized by convective precipitation, which can be the subject of some difficulties. Nevertheless, this issue can be solved by using station-based data (usually available in real time from different meteorological offices) or satellite measurements. The performance of our simple model was found to be weaker for the June extremes floods, compared to the April ones, but together with the precipitation that

fell prior to the floods, our model was still able to predict ~75% of the total magnitude of the June 2013 flood, even though the predicted discharge for this particular event was still underestimated by 25%. This might be due to the fact that extreme floods during summer months are the direct result of both the previous months' conditions as well as extreme heavy rainfall, while for winter and spring months the extreme floods are the results of snow cover, snowmelt, and incremental warming, making the performance of the model much better because of longer memory. The June 2013 flood event was a real test also for the operational European Flood Awareness System (EFAS), which did perform well in most of the affected areas, even though the severity of the event was somewhat underestimated (Pappenberger et al. 2013).

Furthermore, the information regarding the specific atmospheric synoptic state (blocking-like structure) that persisted over the same area for more than 15 days and that was favorable to high streamflows over Elbe's catchment area could have been also considered as a warning signal regarding a potential flood at the beginning of June 2013. Also, the use of soil moisture information from the previous month as a potential predictor proves to be an important factor in improving the forecast skill. Although our analysis was restricted to a particular basin, a similar forecast scheme could be also applied for other rivers. The advantages of this methodology, compared to other flood prediction products available for Europe (Alfieri et al. 2013) or globally (Werner et al. 2013; Candogan Yossef et al. 2013), are 1) it is inexpensive in terms of computational and human resources; 2) it does not require the use of a hydrological model, which is mostly not freely available and has high computational costs; and 3) it does not require access to operational ensemble forecast data, like most of the available flood prediction products do. Therefore, using a simple and computationally inexpensive statistical model, one can anticipate to a certain degree extreme upcoming floods, based on the antecedent climate conditions over specific regions. Finally, since the concept can be used as an early warning system for floods, the potential societal benefits in terms of limiting life and monetary loss are enormous.

REFERENCES

Alfieri, L., P. Burek, E. Dutra, B. Krzeminski, D. Muraro, J. Thielen, and F. Pappenberger, 2013: GloFAS—Global ensemble streamflow forecasting and flood early warning. *Hydrol. Earth Syst. Sci.,* **17,** 1161–1175, doi:10.5194/hess-17-1161-2013.

Belz, J. U., P. Burek, H. Matthäus, B. Rudolf, S. Vollmer, and W. Wiechmann, 2006: Das Hochwasser der Elbe im Frühjahr 2006 (in German). BfG-1514, Bundesanstalt fürGewässerkunde, Koblenz, Germany, 43 pp. [Available online at http://undine.bafg.de/servlet/is/12448/BfG_Bericht_HW2006.pdf.]

Berg, A. A., and K. A. Mulroy, 2006: Streamflow predictability in the Saskatchewan/Nelson River basin given macroscale estimates of the initial soil moisture status. *Hydrol. Sci.,* **51,** 642–654, doi:10.1623/hysj.51.4.642.

——, J. S. Famiglietti, J. P. Walker, and P. R. Houser, 2003: Impact of bias correction to reanalysis products on simulations of North American soil moisture and hydrological fluxes. *J. Geophys. Res.,* **108,** 4490, doi:10.1029/2002JD003334.

Candogan Yossef, N., H. Winsemius, A. Weerts, R. van Beek, and M. F. P. Bierkens, 2013: Skill of a global seasonal streamflow forecasting system, relative roles of initial conditions and meteorological forcing. *Water Resour. Res.,* **49,** 4687–4699, doi:10.1002/wrcr.20350.

Compo, G. P., J. S. Whitaker, and P. D. Sardeshmukh, 2006: Feasibility of a 100-year reanalysis using only surface pressure data. *Bull. Amer. Meteor. Soc.,* **87,** 175–190, doi:10.1175/BAMS-87-2-175.

——, and Coauthors, 2011: The Twentieth Century Reanalysis Project. *Quart. J. Roy. Meteor. Soc.,* **137,** 1–28, doi:10.1002/qj.776.

Cullen, H. M., A. Kaplan, P. Arkin, and P. B. DeMenocal, 2002: Impact of the North Atlantic Oscillation on Middle Eastern climate and streamflow. *Climatic Change,* **55,** 315–338, doi:10.1023/A:1020518305517.

Dee, D. P., and Coauthors, 2011: The ERA-Interim reanalysis: Configuration and performance of the data assimilation system. *Quart. J. Roy. Meteor. Soc.,* **137,** 553–597, doi:10.1002/qj.828.

Delworth, T., and S. Manabe, 1993: Climate variability and land surface processes. *Adv. Water Resour.,* **16,** 3–20, doi:10.1016/0309-1708(93)90026-C.

Dettinger, M. D., and H. F. Diaz, 2000: Global characteristics of streamflow seasonality. *J. Hydrometeor.,* **1,** 289–310, doi:10.1175/1525-7541(2000)001<0289:GCOSFS>2.0.CO;2.

Deutscher Wetterdienst, 2013a: Extreme Bodenfeuchte wie seit 50 Jahren nicht mehr. DWD press release, 31 May.

——, 2013b: The weather in Germany in May. DWD press release, 28 May.

Dirmeyer, P. A., and K. L. Brubaker, 1999: Contrasting evaporative moisture sources during the drought of 1988 and the flood of 1993. *J. Geophys. Res.,* **104,** 19 383–19 397, doi:10.1029/1999JD900222.

Gámiz-Fortis, S. R., M. J. Esteban-Parra, R. M. Trigo, and Y. Castro-Díez, 2010: Potential predictability of an Iberian river flow based on its relationship with previous winter global SST. *J. Hydrol.,* **385,** 143–149, doi:10.1016/j.jhydrol.2010.02.010.

Haylock, M. R., N. Hofstra, A. M. G. Klein Tank, E. J. Klok, P. D. Jones, and M. New, 2008: A European daily high-resolution gridded data set of surface temperature and precipitation for 1950–2006. *J. Geophys. Res.,* **113,** D20119, doi:10.1029/2008JD010201.

Ionita, M., G. Lohmann, and N. Rimbu, 2008: Prediction of Elbe discharge based on stable teleconnections with winter global temperature and precipitation. *J. Climate,* **21,** 6215–6226, doi:10.1175/2008JCLI2248.1.

Kalnay, E., and Coauthors, 1996: The NCEP/NCAR 40-Year Reanalysis Project. *Bull. Amer. Meteor. Soc.,* **77,** 437–470, doi:10.1175/1520-0477(1996)077<0437:TNYRP>2.0.CO;2.

Kirono, D. G. C., F. H. S. Chiew, and D. M. Kent, 2010: Identification of best predictors for forecasting seasonal rainfall and runoff in Australia. *Hydrol. Processes,* **24,** 1237–1247, doi:10.1002/hyp.7585.

Kistler, R., and Coauthors, 2001: The NCEP–NCAR 50-year reanalysis: Monthly means CD-ROM and documentation. *Bull. Amer. Meteor. Soc.,* **82,** 247–267, doi:10.1175/1520-0477(2001)082<0247:TNNYRM>2.3.CO;2.

Koster, R. D., S. P. P. Mahanama, B. Livneh, D. P. Lettenmaier, and R. H. Reichle, 2010: Skill in streamflow forecasts derived from large-scale estimates of soil moisture and snow. *Nat. Geosci.,* **3,** 613–616, doi:10.1038/ngeo944.

Liu, L., R. Zhang, and Z. Zuo, 2014: Intercomparison of spring soil moisture among multiple reanalysis data sets over eastern China. *J. Geophys. Res. Atmos.,* **119,** 54–64, doi:10.1002/2013JD020940.

Lohmann, G., N. Rimbu, and M. Dima, 2005: Where can the Arctic Oscillation be reconstructed? Towards a reconstruction of climate modes based on stable teleconnections. *Climate Past Discuss.,* **1,** 17–56, doi:10.5194/cpd-1-17-2005.

Mahanama, S. P. P., R. D. Koster, R. H. Reichle, and L. Zubair, 2008: The role of soil moisture initialization in subseasonal and seasonal streamflow prediction—A case study in Sri Lanka. *Adv. Water Resour.,* **31,** 1333–1343, doi:10.1016/j.advwatres.2008.06.004.

Manabe, S., and T. Delworth, 1990: The temporal variability of soil wetness and its impact on climate. *Climatic Change,* **16,** 185–192, doi:10.1007/BF00134656.

McKee, T. B., N. J. Doesken, and J. Kliest, 1993: The relationship of drought frequency and duration to time scales. *Proc. Eighth Conf. on Applied Climatology,* Anaheim, CA, Amer. Meteor. Soc., 179–184.

Mudelsee, M., M. Börngen, G. Tetzlaff, and U. Grünewald, 2004: Extreme floods in central Europe over the past 500 years: Role of cyclone pathway "Zugstrasse Vb." *J. Geophys. Res.,* **109,** D23101, doi:10.1029/2004JD005034.

Munich RE, 2013: Floods dominate natural catastrophe statistics in the first half of 2013. Press release, 9 July.

Pan, H.-L., and L. Mahrt, 1987: Interaction between soil hydrology and boundary-layer development. *Bound.-Layer Meteor.,* **38,** 185–202, doi:10.1007/BF00121563.

Pappenberger, F., and Coauthors, 2013: Floods in central Europe in June 2013. *ECMWF Newsletter,* No. 136, ECMWF, Reading, United Kingdom, 9–11.

Puffahrt, O., 2008: Historische und neuzeitliche Hochwassergeschehnisse im Raum Hitzacker. NLWKN Rep., 102 pp. [Available online at www.nlwkn.niedersachsen.de/download/24595/Band_2_zum_Hochwasserschutz_fuer_Hitzacker_und_die_Jeetzelniederung_Historische_und_neuzeitliche_Hochwassergeschehnisse_im_Raum_Hitzacker.pdf.]

Reichle, R. H., and R. D. Koster, 2003: Assessing the impact of horizontal error correlations in background fields on soil moisture estimation. *J. Hydrometeor.,* **4,** 1229–1242, doi:10.1175/1525-7541(2003)004<1229:ATIOHE>2.0.CO;2.

——, ——, G. J. M. De Lannoy, B. A. Forman, Q. Liu, S. Mahanama, and A. Toure, 2011: Assessment and enhancement of MERRA land surface hydrology estimates. *J. Climate,* **24,** 6322–6338, doi:10.1175/JCLI-D-10-05033.1.

Rex, D. F., 1950: Blocking action in the middle troposphere and its effect upon regional climate. *Tellus,* **2,** 275–301, doi:10.1111/j.2153-3490.1950.tb00339.x.

Rienecker, M. M., and Coauthors, 2011: MERRA: NASA's Modern-Era Retrospective Analysis for Research and Applications. *J. Climate,* **24,** 3624–3648, doi:10.1175/JCLI-D-11-00015.1.

Rimbu, N., M. Dima, G. Lohmann, and I. Musat, 2005: Seasonal prediction of Danube flow variability based on stable

teleconnection with sea surface temperature. *Geophys. Res. Lett., 32,* L21704, doi:10.1029/2005GL024241.

Scherrer, S. C., M. Croci-Maspoli, C. Schwierz, and C. Appenzeller, 2006: Two-dimensional indices of atmospheric blocking and their statistical relationship with winter climate patterns in the Euro-Atlantic region. *Int. J. Climatol., 26,* 233–249, doi:10.1002/joc.1250.

Sillmann, J., and M. Croci-Maspoli, 2009: Present and future atmospheric blocking and its impact on European mean and extreme climate. *Geophys. Res. Lett., 36,* L1072, doi:10.1029/2009GL038259.

Svensson, C., and C. Prudhomme, 2005: Prediction of British summer river flows using winter predictors. *Theor. Appl. Climatol., 82,* 1–15, doi:10.1007/s00704-005-0124-5.

Tibaldi, S., and F. Molteni, 1990: On the operational predictability of blocking. *Tellus, 42A,* 343–365, doi:10.1034/j.1600-0870.1990.t01-2-00003.x.

Tootle, G. A., and T. C. Piechota, 2006: Relationships between Pacific and Atlantic ocean sea surface temperatures and U.S. streamflow variability. *Water Resour. Res., 42,* W07411, doi:10.1029/2005WR004184.

Trigo, R. M., D. Pozo-Vázquez, T. J. Osborn, Y. Castro-Diez, S. Gámiz-Fortis, and M. J. Esteban-Parra, 2004: North Atlantic Oscillation influence on precipitation, river flow and water resources in the Iberian Peninsula. *Int. J. Climatol., 24,* 925–944, doi:10.1002/joc.1048.

Vinnikov, K. Y., and I. B. Yeserkepova, 1991: Soil moisture: Empirical data and model results. *J. Climate, 4,* 66–79, doi:10.1175/1520-0442(1991)004<0066:SMEDAM>2.0.CO;2.

von Storch, H., and F. W. Zwiers, 1999: *Statistical Analysis in Climate Research.* Cambridge University Press, 484 pp.

Wedgbrow, C. S., R. L. Wilby, H. R. Fox, and G. O'Hare, 2002: Prospects for seasonal forecasting of summer drought and low river flow anomalies in England and Wales. *Int. J. Climatol., 22,* 219–236, doi:10.1002/joc.735.

Werner, M., J. Schellekens, P. Gijsbers, M. van Dijk, O. van den Akker, and K. Heynert, 2013: The Delft-FEWS flow forecasting system. *Environ. Modell. Software, 40,* 65–77, doi:10.1016/j.envsoft.2012.07.010.

Whitaker, J. S., G. P. Compo, X. Wei, and T. M. Hamill, 2004: Reanalysis without radiosondes using ensemble data assimilation. *Mon. Wea. Rev., 132,* 1190–1200, doi:10.1175/1520-0493(2004)132<1190:RWRUED>2.0.CO;2.

Wilby, R. L., C. S. Wedgbrow, and H. R. Fox, 2004: Seasonal predictability of the summer hydrometeorology of the River Thames, UK. *J. Hydrol., 295,* 1–16, doi:10.1016/j.jhydrol.2004.02.015.

Wilks, D. S., 1995: *Statistical Methods in the Atmospheric Sciences.* International Geophysics Series, Vol. 59, Academic Press, 464 pp.

Wood, A. W., and D. P. Lettenmaier, 2006: A test bed for new seasonal hydrologic forecasting approaches in the western United States. *Bull. Amer. Meteor. Soc., 87,* 1699–1712, doi:10.1175/BAMS-87-12-1699.

——, E. P. Maurer, A. Kumar, and D. P. Lettenmaier, 2002: Long-range experimental hydrologic forecasting for the eastern United States. *J. Geophys. Res., 107,* 4429, doi:10.1029/2001JD000659.

——, A. Kumar, and D. P. Lettenmaier, 2005: A retrospective assessment of National Centers for Environmental Prediction climate model–based ensemble hydrologic forecasting in the western United States. *J. Geophys. Res., 110,* D04105, doi:10.1029/2004JD004508.

Zhao, M., S. W. Running, and R. R. Nemani, 2006: Sensitivity of Moderate Resolution Imaging Spectroradiometer (MODIS) terrestrial primary production to the accuracy of meteorological reanalysis. *J. Geophys. Res., 111,* G01002, doi:10.1029/2004JG000004.